# ANALYTICAL SOLUTION TO THE SCATTERING OF PLANE P WAVES BY ALLUVIAL VALLEYS CONTAINING MULTIPLE CIRCULAR-ARC LAYERS

**ZHANG Yushan[1] and YANG Caihong[2]**

[1] *Associate Professor, China Earthquake Disaster Prevention Center, Beijing, China*
[2] *Assistant Professor, China Earthquake Disaster Prevention Center, Beijing, China*
*Email: hyszhang@163.com,yangch19740815@163.com*

**ABSTRACT :**

By the method of Fourier-Bessel series expansion of wave functions, presented is an analytical solution to the stationary dynamic response of alluvial valley containing arbitrary number of circular-arc layers incident by plane P wave. Taking the three-layer valleys as examples and using the spatial distributions of amplitude and phase difference of stationary ground motion, the influences of the layering of valley deposit media on the ground motion are studied in a broad frequency band.

**KEYWORDS:** Alluvial valley containing multiple circular-arc layers, Plane P wave, Scattering, Analytical solution

## 1. INTRODUCTION

The study of analytical solution to the problem of seismic wave scattering and diffraction by regular alluvial valley is an important topic in earthquake engineering. Using Fourier-Bessel series expansion and Mathieu series expansion to wave functions, Trifunac (Trifunac, 1971) and Wong and Trifunac (Wong and Trifunac, 1974) obtained the analytical solution for the SH wave scattering by the two-dimension valley with semi-circular and semi-ellipse section, respectively. Thereafter, the method of Fourier-Bessel series expansion method was used to solve the scattering and diffraction of different types of waves by different valleys with circular-arc section (Todorovska and Lee, 1991; Liang etc, 2001, 2003, 2006; Li etc, 2005; Li and Zhao, 2004; Yuan and Liao, 1995).

However, the above studies all presumed that the deposit in the valley contains single medium. By the method used by Todorovska and Lee (1991), Liang etc (2000, 2001, 2003) solved the scatterings of body waves by two-dimension (2D) layered valley with shallow-arc section, and studied the influences of the sequence of alluvial layers, the stiffness and thickness of soft interlayer, etc., on ground motion. But due to complexity of the problem, their studies considered the valley with only two layers. In this paper, firstly, by using the same method as Todorovska and Lee (1991), deduced is the analytical solution to the scattering of P wave by the 2D valley with shallow-arc section which contains arbitrary number of layers. And then, with the three-layered valley as example, the influence of the layering of deposit media in the valley on the stationary ground motion is discussed in a broad frequency band.

## 2. MODEL

The model of multi-layered alluvial valley with shallow-arc section is shown in Fig.1. There are $L$ layers of alluvial media above the half space, $l = 0,1,2,\ldots,L\text{-}1$, with the sequential number of half-space medium being $L$, therefore, there are altogether $L+1$ kinds of media in the model. The boundaries between any two adjacent media are all shallow arcs, with their centers all being at the point of $O_1$. The half-width, the depth, and the radius of each arc are denoted by $a_l$, $h_l$, and $b_l$, respectively. The height of center $O_1$ is $h_0=b_1-h_1$. The shear-wave

velocity, the density, and the Poisson's ratio of each medium are denoted by $c_s^{(l)}$, $\rho^{(l)}$, and $\nu^{(l)}$, respectively, so the corresponding Lame constants and the dilatational-wave velocity are

$$\mu^{(l)} = \rho^{(l)}[c_s^{(l)}]^2, \lambda^{(l)} = 2\nu^{(l)}\mu^{(l)}/(1-2\nu^{(l)}), c_p^{(l)} = \sqrt{(\lambda^{(l)}+2\mu^{(l)})/\rho^{(l)}} \tag{2.1}$$

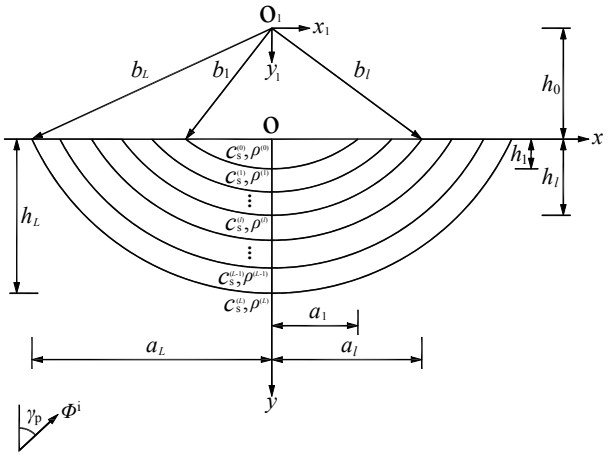


Figure 1 The model of alluvial valley

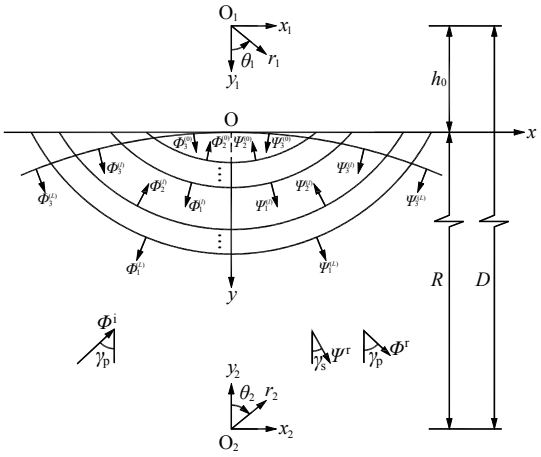


Figure 2 The scattering of waves

The incident P wave is harmonic plane wave, with its frequency being $\omega$ and incident angle $\gamma_p$. In the coordinate system $x$-$y$, its potential function with time factor exp(-i$\omega t$) being omitted is

$$\Phi^i(x,y) = \exp[ik_p^{(L)}(x\sin\gamma_p - y\cos\gamma_p)] \tag{2.2}$$

where i is the imaginary unit, $i = \sqrt{-1}$, and $k_p^{(L)}$ is the P wave number of half-space medium. Similarly,

$$k_p^{(l)} = \omega/c_p^{(l)}, k_s^{(l)} = \omega/c_s^{(l)} \tag{2.3}$$

are the P and the S wave numbers of the $l$-th medium, respectively. In the stationary case, the potentials of P and SV waves satisfy the following Poisson's equation

$$\begin{aligned} \nabla^2\Phi + k_p^2\Phi = 0 \\ \nabla^2\Psi + k_s^2\Psi = 0 \end{aligned} \tag{2.4}$$

The boundary conditions contain the zero-stress condition on the surface

$$\left.\begin{Bmatrix} t_{yy}^{(l)}(x,y) \\ t_{xy}^{(l)}(x,y) \end{Bmatrix}\right|_{y=0} = 0, \quad l = 0,1,2,...,L \tag{2.5a}$$

and the continuity conditions at the $l$-th arc boundary

$$\left.\begin{Bmatrix} u_r^{(l-1)}(r_1,\theta_1) \\ u_\theta^{(l-1)}(r_1,\theta_1) \end{Bmatrix}\right|_{r_1=b_l} = \left.\begin{Bmatrix} u_r^{(l)}(r_1,\theta_1) \\ u_\theta^{(l)}(r_1,\theta_1) \end{Bmatrix}\right|_{r_1=b_l} \tag{2.5b}$$

$$\left\{\begin{matrix} t_{rr}^{(l-1)}(r_1,\theta_1) \\ t_{r\theta}^{(l-1)}(r_1,\theta_1) \end{matrix}\right\}\Bigg|_{r_1=b_l} = \left\{\begin{matrix} t_{rr}^{(l)}(r_1,\theta_1) \\ t_{r\theta}^{(l)}(r_1,\theta_1) \end{matrix}\right\}\Bigg|_{r_1=b_l} \tag{2.5c}$$

where $t$ denotes the stress, and $u$ the displacement.

## 3. POTENTIAL FUNCTIONS OF SCATTERING WAVES

Before solving out the displacement field, in order to conveniently applying the surface zero-stress condition, the method used by Todorovska and Lee (1991) is still used here, i.e., a circular arc with very big radius is introduced to approximately simulate the level surface of the half space. As shown in Fig.2, the radius of the arc is $R$, and it centers at the point of $O_2$. And accordingly, in the polar system $r_2$-$\theta_2$ shown in Fig.2, zero-stress condition (2.5a) is changed into

$$\left\{\begin{matrix} t_{rr}^{(l)}(r_2,\theta_2) \\ t_{r\theta}^{(l)}(r_2,\theta_2) \end{matrix}\right\}\Bigg|_{r_2=R} = 0, \quad l = 0,1,2,...,L \tag{2.5a}$$

### *3.1 The Potential Functions of Scattering Waves in the Half Space*

In the half space, the free-field waves include the incident P wave $\Phi^{\mathrm{i}}$, the reflected P wave $\Phi^{\mathrm{r}}$, and the reflected SV wave $\Psi^{\mathrm{r}}$. Referring Zhang (2008), the potentials of the free-field P and SV waves can be expressed in coordinate system $r_1$-$\theta_1$ by

$$\left\{\begin{matrix} \Phi^{\mathrm{i+r}}(r_1,\theta_1) \\ \Psi^{\mathrm{r}}(r_1,\theta_1) \end{matrix}\right\} = \sum_{n=0}^{\infty}\left\{\begin{matrix} \mathrm{J}_n(k_{\mathrm{p}}^{(L)}r_1)(A_{0,n}\cos n\theta_1 + B_{0,n}\sin n\theta_1) \\ \mathrm{J}_n(k_{\mathrm{s}}^{(L)}r_1)(C_{0,n}\sin n\theta_1 + D_{0,n}\cos n\theta_1) \end{matrix}\right\} \tag{3.1}$$

where

$$\left\{\begin{matrix} A_{0,n} \\ B_{0,n} \end{matrix}\right\} = \varepsilon_n \mathrm{i}^n[\pm(-1)^n \exp(\mathrm{i}k_{\mathrm{p}}^{(L)}h_0\cos\gamma_{\mathrm{p}}) + w_1\exp(-\mathrm{i}k_{\mathrm{p}}^{(L)}h_0\cos\gamma_{\mathrm{p}})]\left\{\begin{matrix} \cos n\gamma_{\mathrm{p}} \\ \sin n\gamma_{\mathrm{p}} \end{matrix}\right\} \tag{3.2}$$

$$\left\{\begin{matrix} C_{0,n} \\ D_{0,n} \end{matrix}\right\} = \varepsilon_n \mathrm{i}^n w_2 \exp(-\mathrm{i}k_{\mathrm{s}}^{(L)}h_0\cos\gamma_{\mathrm{s}})]\left\{\begin{matrix} \sin n\gamma_{\mathrm{s}} \\ \cos n\gamma_{\mathrm{s}} \end{matrix}\right\} \tag{3.3}$$

In equation (3.2) and (3.3), if $n = 0$, then $\varepsilon_n = 1$, while if $n > 0$, then $\varepsilon_n = 2$. In the half space, apart from the above free-field waves, there also exist the scattering waves due to the presence of the arc-shaped multi-layered valley, as shown in Fig.2, where $\Phi_1^{(L)}$ and $\Psi_1^{(L)}$ represent the cylindrical waves radiating from the center $O_1$, while $\Phi_3^{(L)}$ and $\Psi_3^{(L)}$ describe the cylindrical standing waves residing between the "curved" surface and the $L$-th small arc boundary. In the coordinate systems of $r_1$-$\theta_1$ and $r_2$-$\theta_2$, these two kinds of waves have the following Fourier-Bessel series expressions respectively

$$\left\{\begin{matrix} \Phi_1^{(L)}(r_1,\theta_1) \\ \Psi_1^{(L)}(r_1,\theta_1) \end{matrix}\right\} = \sum_{n=0}^{\infty}\left\{\begin{matrix} \mathrm{H}_n^{(1)}(k_{\mathrm{p}}^{(L)}r_1)(A_{11,n}^{(L)}\cos n\theta_1 + B_{11,n}^{(L)}\sin n\theta_1) \\ \mathrm{H}_n^{(1)}(k_{\mathrm{s}}^{(L)}r_1)(C_{11,n}^{(L)}\sin n\theta_1 + D_{11,n}^{(L)}\cos n\theta_1) \end{matrix}\right\} \tag{3.4}$$

$$\begin{Bmatrix} \Phi_3^{(L)}(r_2,\theta_2) \\ \Psi_3^{(L)}(r_2,\theta_2) \end{Bmatrix} = \sum_{m=0}^{\infty} \begin{Bmatrix} \mathrm{J}_m(k_\mathrm{p}^{(L)} r_2)(A_{32,m}^{(L)} \cos m\theta_2 + B_{32,m}^{(L)} \sin m\theta_2) \\ \mathrm{J}_m(k_\mathrm{s}^{(L)} r_2)(C_{32,m}^{(L)} \sin m\theta_2 + D_{32,m}^{(L)} \cos m\theta_2) \end{Bmatrix} \tag{3.5}$$

By the interior Graf addition formula (Zhang, 2008), the above wave functions can be expressed in the alternative coordinate system as follows

$$\begin{Bmatrix} \Phi_1^{(L)}(r_2,\theta_2) \\ \Psi_1^{(L)}(r_2,\theta_2) \end{Bmatrix} = \sum_{m=0}^{\infty} \begin{Bmatrix} \mathrm{J}_m(k_\mathrm{p}^{(L)} r_2)(A_{12,m}^{(L)} \cos m\theta_2 + B_{12,m}^{(L)} \sin m\theta_2) \\ \mathrm{J}_m(k_\mathrm{s}^{(L)} r_2)(C_{12,m}^{(L)} \sin m\theta_2 + D_{12,m}^{(L)} \cos m\theta_2) \end{Bmatrix} \tag{3.6}$$

$$\begin{Bmatrix} \Phi_3^{(L)}(r_1,\theta_1) \\ \Psi_3^{(L)}(r_1,\theta_1) \end{Bmatrix} = \sum_{n=0}^{\infty} \begin{Bmatrix} \mathrm{J}_n(k_\mathrm{p}^{(L)} r_1)(A_{31,n}^{(L)} \cos n\theta_1 + B_{31,n}^{(L)} \sin n\theta_1) \\ \mathrm{J}_n(k_\mathrm{s}^{(L)} r_1)(C_{31,n}^{(L)} \sin n\theta_1 + D_{31,n}^{(L)} \cos n\theta_1) \end{Bmatrix} \tag{3.7}$$

where

$$\begin{Bmatrix} A_{12,m}^{(L)} \\ B_{12,m}^{(L)} \\ C_{12,m}^{(L)} \\ D_{12,m}^{(L)} \end{Bmatrix} = \sum_{n=0}^{\infty} \begin{Bmatrix} \mathrm{E}_{mn}^{(3)+}(k_\mathrm{p}^{(L)} D) A_{11,n}^{(L)} \\ \mathrm{E}_{mn}^{(3)-}(k_\mathrm{p}^{(L)} D) B_{11,n}^{(L)} \\ \mathrm{E}_{mn}^{(3)-}(k_\mathrm{s}^{(L)} D) C_{11,n}^{(L)} \\ \mathrm{E}_{mn}^{(3)+}(k_\mathrm{s}^{(L)} D) D_{11,n}^{(L)} \end{Bmatrix} \tag{3.8a}$$

$$\begin{Bmatrix} A_{31,n}^{(L)} \\ B_{31,n}^{(L)} \\ C_{31,n}^{(L)} \\ D_{31,n}^{(L)} \end{Bmatrix} = \sum_{m=0}^{\infty} \begin{Bmatrix} \mathrm{E}_{nm}^{(1)+}(k_\mathrm{p}^{(L)} D) A_{32,m}^{(L)} \\ \mathrm{E}_{nm}^{(1)-}(k_\mathrm{p}^{(L)} D) B_{32,m}^{(L)} \\ \mathrm{E}_{nm}^{(1)-}(k_\mathrm{s}^{(L)} D) C_{32,m}^{(L)} \\ \mathrm{E}_{nm}^{(1)+}(k_\mathrm{s}^{(L)} D) D_{32,m}^{(L)} \end{Bmatrix} \tag{3.8b}$$

$$\mathrm{E}_{jk}^{(q)\pm}(x) = \frac{\varepsilon_j}{2}[\ell_{j+k}^{(q)}(x) \pm (-1)^k \ell_{j-k}^{(q)}(x)] \tag{3.9}$$

In equation (3.9), if $q$ = 1, then $\ell_n^{(q)}(x)$ denotes the 1st kind Bessel function $\mathrm{J}_n(x)$, while if $q$ = 1, then $\ell_n^{(q)}(x)$ denotes the 1st kind Hankel function $\mathrm{H}_n^{(1)}(x)$. And in equation (3.8), $D$ is the distance between the center $\mathrm{O}_1$ and $\mathrm{O}_2$, as shown in Fig.2.

### *3.2 The Potential Functions of Scattering Waves in the Deposits*

In the $l$-th layer, there exist two kinds of cylindrical standing waves, i.e. the scattering waves of $\Phi_2^{(l)}$ and $\Psi_2^{(l)}$, and these of $\Phi_3^{(l)}$ and $\Psi_3^{(l)}$. In addition, there also exits the cylindrical waves radiating from center $\mathrm{O}_1$, $\Phi_1^{(l)}$ and $\Psi_1^{(l)}$, however, when $l$ = 0, i.e. in the upmost deposit, this kind of cylindrical radiating wave disappears, as shown in Fig.2. In the coordinate systems $r_1$-$\theta_1$ and $r_2$-$\theta_2$, the potentials of these scattering waves have the following expressions

$$\begin{Bmatrix} \Phi_1^{(l)}(r_1,\theta_1) \\ \Psi_1^{(l)}(r_1,\theta_1) \end{Bmatrix} = \sum_{n=0}^{\infty} \begin{Bmatrix} \mathrm{H}_n^{(1)}(k_\mathrm{p}^{(l)} r_1)(A_{11,n}^{(l)} \cos n\theta_1 + B_{11,n}^{(l)} \sin n\theta_1) \\ \mathrm{H}_n^{(1)}(k_\mathrm{s}^{(l)} r_1)(C_{11,n}^{(l)} \sin n\theta_1 + D_{11,n}^{(l)} \cos n\theta_1) \end{Bmatrix} \tag{3.10}$$

$$\begin{Bmatrix}\Phi_2^{(l)}(r_1,\theta_1)\\ \Psi_2^{(l)}(r_1,\theta_1)\end{Bmatrix}=\sum_{n=0}^{\infty}\begin{Bmatrix}\mathrm{J}_n(k_{\mathrm{p}}^{(l)}r_1)(A_{21,n}^{(l)}\cos n\theta_1+B_{21,n}^{(l)}\sin n\theta_1)\\ \mathrm{J}_n(k_{\mathrm{s}}^{(l)}r_1)(C_{21,n}^{(l)}\sin n\theta_1+D_{21,n}^{(l)}\cos n\theta_1)\end{Bmatrix} \tag{3.11}$$

$$\begin{Bmatrix}\Phi_3^{(l)}(r_2,\theta_2)\\ \Psi_3^{(l)}(r_2,\theta_2)\end{Bmatrix}=\sum_{m=0}^{\infty}\begin{Bmatrix}\mathrm{J}_m(k_{\mathrm{p}}^{(l)}r_2)(A_{32,m}^{(l)}\cos m\theta_2+B_{32,m}^{(l)}\sin m\theta_2)\\ \mathrm{J}_m(k_{\mathrm{s}}^{(l)}r_2)(C_{32,m}^{(l)}\sin m\theta_2+D_{32,m}^{(l)}\cos m\theta_2)\end{Bmatrix} \tag{3.12}$$

By the Graf addition formula, the expressions of the above wave functions in the alternative coordinate system are

$$\begin{Bmatrix}\Phi_1^{(l)}(r_2,\theta_2)\\ \Psi_1^{(l)}(r_2,\theta_2)\end{Bmatrix}=\sum_{m=0}^{\infty}\begin{Bmatrix}\mathrm{J}_m(k_{\mathrm{p}}^{(l)}r_2)(A_{12,m}^{(l)}\cos m\theta_2+B_{12,m}^{(l)}\sin m\theta_2)\\ \mathrm{J}_m(k_{\mathrm{s}}^{(l)}r_2)(C_{12,m}^{(l)}\sin m\theta_2+D_{12,m}^{(l)}\cos m\theta_2)\end{Bmatrix} \tag{3.13}$$

$$\begin{Bmatrix}\Phi_2^{(l)}(r_2,\theta_2)\\ \Psi_2^{(l)}(r_2,\theta_2)\end{Bmatrix}=\sum_{m=0}^{\infty}\begin{Bmatrix}\mathrm{J}_m(k_{\mathrm{p}}^{(l)}r_2)(A_{22,m}^{(l)}\cos m\theta_2+B_{22,m}^{(l)}\sin m\theta_2)\\ \mathrm{J}_m(k_{\mathrm{s}}^{(l)}r_2)(C_{22,m}^{(l)}\sin m\theta_2+D_{22,m}^{(l)}\cos m\theta_2)\end{Bmatrix} \tag{3.14}$$

$$\begin{Bmatrix}\Phi_3^{(l)}(r_1,\theta_1)\\ \Psi_3^{(l)}(r_1,\theta_1)\end{Bmatrix}=\sum_{n=0}^{\infty}\begin{Bmatrix}\mathrm{J}_n(k_{\mathrm{p}}^{(l)}r_1)(A_{31,n}^{(l)}\cos n\theta_1+B_{31,n}^{(l)}\sin n\theta_1)\\ \mathrm{J}_n(k_{\mathrm{s}}^{(l)}r_1)(C_{31,n}^{(l)}\sin n\theta_1+D_{31,n}^{(l)}\cos n\theta_1)\end{Bmatrix} \tag{3.15}$$

where

$$\begin{Bmatrix}A_{12,m}^{(l)}\\ B_{12,m}^{(l)}\\ C_{12,m}^{(l)}\\ D_{12,m}^{(l)}\end{Bmatrix}=\sum_{n=0}^{\infty}\begin{Bmatrix}\mathrm{E}_{mn}^{(3)+}(k_{\mathrm{p}}^{(l)}D)A_{11,n}^{(l)}\\ \mathrm{E}_{mn}^{(3)-}(k_{\mathrm{p}}^{(l)}D)B_{11,n}^{(l)}\\ \mathrm{E}_{mn}^{(3)-}(k_{\mathrm{s}}^{(l)}D)C_{11,n}^{(l)}\\ \mathrm{E}_{mn}^{(3)+}(k_{\mathrm{s}}^{(l)}D)D_{11,n}^{(l)}\end{Bmatrix} \tag{3.16a}$$

$$\begin{Bmatrix}A_{22,m}^{(l)}\\ B_{22,m}^{(l)}\\ C_{22,m}^{(l)}\\ D_{22,m}^{(l)}\end{Bmatrix}=\sum_{n=0}^{\infty}\begin{Bmatrix}\mathrm{E}_{mn}^{(1)+}(k_{\mathrm{p}}^{(l)}D)A_{21,n}^{(l)}\\ \mathrm{E}_{mn}^{(1)-}(k_{\mathrm{p}}^{(l)}D)B_{21,n}^{(l)}\\ \mathrm{E}_{mn}^{(1)-}(k_{\mathrm{s}}^{(l)}D)C_{21,n}^{(l)}\\ \mathrm{E}_{mn}^{(1)+}(k_{\mathrm{s}}^{(l)}D)D_{21,n}^{(l)}\end{Bmatrix} \tag{3.16b}$$

$$\begin{Bmatrix}A_{31,n}^{(l)}\\ B_{31,n}^{(l)}\\ C_{31,n}^{(l)}\\ D_{31,n}^{(l)}\end{Bmatrix}=\sum_{m=0}^{\infty}\begin{Bmatrix}\mathrm{E}_{nm}^{(1)+}(k_{\mathrm{p}}^{(l)}D)A_{32,m}^{(l)}\\ \mathrm{E}_{nm}^{(1)-}(k_{\mathrm{p}}^{(l)}D)B_{32,m}^{(l)}\\ \mathrm{E}_{nm}^{(1)-}(k_{\mathrm{s}}^{(l)}D)C_{32,m}^{(l)}\\ \mathrm{E}_{nm}^{(1)+}(k_{\mathrm{s}}^{(l)}D)D_{32,m}^{(l)}\end{Bmatrix} \tag{3.16c}$$

When $l$=0, the cylindrical radiating waves represented by equation (3.10) and (3.13) do not exist, and thus

$$\begin{Bmatrix}A_{11,n}^{(0)}\\ B_{11,n}^{(0)}\end{Bmatrix}=\begin{Bmatrix}C_{11,n}^{(0)}\\ D_{11,n}^{(0)}\end{Bmatrix}=0\,,\quad \begin{Bmatrix}A_{12,m}^{(0)}\\ B_{12,m}^{(0)}\end{Bmatrix}=\begin{Bmatrix}C_{12,m}^{(0)}\\ D_{12,m}^{(0)}\end{Bmatrix}=0 \tag{3.17}$$

By introducing the boundary conditions, the undetermined coefficients, $\{A_{11,n}^{(l)}\}$ etc., in equation (3.4) through (3.7) and equation (3.10) through (3.15) can be solved layer by layer, the detailed deduction can be referred to

Zhang (2008). And thus, the final displacement and stress field can be calculated with these coefficients at hand (Zhang, 2008).

## 4. ANALYSIS OF RESULTS

At first, define the following non-dimension parameter

$$\eta = \frac{2a_L}{\lambda_s^{(L)}} = \frac{\omega a_L}{\pi c_s^{(L)}} \tag{4.1}$$

which is the ratio between the valley width, $2a_L$, and the wavelength of the S wave in the half space, $\lambda_s^{(L)}$. It is an indirect gauge of the frequency of incident wave, i.e. the bigger the value of $\eta$, the shorter the wave length of incident wave $\lambda_p^{(L)}$, and the higher its frequency $\omega$.

The analysis of the convergence of series solution has showed that at least for the incident frequency range $\eta \leq 20$, the series solution presented in this paper can converge to the true solution. As to the value of the radius, $R$, of the big arc that simulates the level ground surface, generally the value of $R = 10^2 b_L \sim 10^5 b_L$ can satisfy the precision requirement. The displacement field of the stationary dynamic response of valley under the harmonic incidence is complex-valued, i.e.

$$u(x,y) = |u(x,y)|\, e^{i\varphi(x,y)} \tag{4.2}$$

where $|u(x,y)|$ is the amplitude of ground motion whose spatial variation describes the distribution of ground motion intensity, and $\varphi(x,y)$ is the phase of ground motion whose spatial variation describes the lag relation of harmonic vibrations between different spatial points. In the following discussion, the ground surface amplitude $|u(x,0)|$ and the absolute value of phase difference $|\Delta\varphi(x,0)|$ will be used as the main parameters to study the influences of the properties of the incident wave and valley on the stationary ground motion.

The three-layered valley will be used as example to study the scattering effect of the layering of the valley deposits on the incident P wave. Three kinds of valley are considered here, i.e., the single-layered valley (V-1), the three-layered normally alluvial valley (V-2), and the three-layered abnormally alluvial valley (V-3), whose geometrical and physical parameters are given in Table 1. The Poisson's ratios of all media are uniformly taken as 0.25. And in V-3 exists soft interlayer.

Table 1 The geometrical and physical parameters of alluvial valleys

| Valley type | Geometrical parameter | Physical parameters | |
|---|---|---|---|
| | $h_1 : h_2 : h_3 : a_3$ | S-wave velocity ratio | Density ratio |
| V-1 | 0.4 : 0.7 : 1.0 : 2 | 200 : 200 : 200 : 400 | 1.6 : 1.6 : 1.6 : 1.8 |
| V-2 | 0.4 : 0.7 : 1.0 : 2 | 150 : 200 : 300 : 400 | 1.5 : 1.6 : 1.7 : 1.8 |
| V-3 | 0.4 : 0.7 : 1.0 : 2 | 200 : 300 : 150 : 400 | 1.6 : 1.7 : 1.5 : 1.8 |

The spatial variations of ground motion amplitudes and phase differences of the above three valleys under the vertical incidence of P wave ($\gamma_p = 0°$) are given in Fig.3, which gives the results for the incident frequencies $\eta$ = 1.0, 4.0, and 16.0. While Fig.4 presents the results corresponding to the inclined incidence ($\gamma_p = 45°$).

From Fig.3 and Fig.4 it can be seen that the ground motion exhibits distinct characteristics of the interference of scattering waves. On the amplitude curves $|u_x| \sim x/a_3$ and $|u_y| \sim x/a_3$ appear some local minima, where the displacement amplitudes are very low, however, at such spatial points, the phase differences reaches their peaks. Such spatial points on the surface are similar to the "wave nodes" of standing waves, whose vibrations cease or

drop to a low level due to the interferences of different traveling waves. At such wave node, the harmonic ground vibration differs from its adjacent point in a relatively high magnitude due to their large phase lag, that is to say, the two adjacent spatial points will undergo comparatively large relative displacement. And thus at such site, as to the horizontal dimension, relatively high tension or compression stress would appear, while as to the vertical dimension, relatively high shear stress would appear and the ground motion would demonstrate torsion effects accordingly.

With the increase of the incident frequency, the wavelength decreases and the incident wave becomes sensitive to the layering of valley deposits, and accordingly, the variation of ground motion becomes complicated, with more wave nodes appearing. And the layering effects can be clearly noticed. As compared with single layered V-1, at some points, the displacement amplitudes of V-2 and V-3 are very high, while very low at the others, which is dependent on the incident frequency. And as to the high-frequency incidences, i.e. $\eta$ = 4.0 and 16.0, on the surface outcrops of the soft interlayer in V-3, there appear distinct peaks on the spatial variation curves of the ground motion amplitudes, indicating significant interference of scattering waves and distinct energy focus occurring in the soft interlayer.

## 5. CONCLUSIONS

In this paper, by the Fourier-Bessel series expansion technique of wave functions, deduced is the analytical solution to the two-dimension scattering problem of the incident plane P wave by the alluvial valley containing arbitrary number of arc-shaped deposit layers. Using this analytical solution, taking the three-layered valley as example and utilizing the ground motion amplitude and phase difference as the parameters, the influence of the layering of the valley deposits on the ground motion is discussed in a broad frequency band. The results demonstrate that as to the multi-layered valley, when the incident frequency is high, the scattering waves exhibit distinct interference and energy focus phenomenon, the ground motion also presents the standing-wave-like properties with many wave nodes appearing, and furthermore, the soft interlayer in the valley can absorb and trap much energy of scattering waves, which leads to the high amplitude of the ground motion on the outcrops of the soft interlayer.

## ACKNOWLEDGMENTS

This work was supported by the National Natural Science Foundation of China (50608066) and Earthquake Science Foundation of China (A07045).

## REFERENCES

Li W.H., Zhao C.G. and Shi P.X. (2005). Scattering of plane P waves by circular-arc alluvial valleys with saturated soil deposits. *Soil Dyn Earthq Engrg* **25,** 997-1014.

Li W.H., Zhao C.G. (2004). Scattering of plane SV waves by circular-arc alluvial valleys with saturated soil deposits. *Chinese Journal of Geophysics* (in Chinese) **47:5,** 911-919.

Liang J.W., Yan L.J., Li J.W., et al. (2001). Response of circular-arc alluvial valleys under incident plane P waves. Rock and Soil Mechanics (in Chinese) **22:2,** 138-143.

Liang J.W., Yan L.J., Qin D., et al. (2003). Dynamic response of circular-arc sedimentary valley site under incident plane SV waves. *China Civil Engineering Journal* (in Chinese) **36:12,** 74-82.

Liang J.W., Zhang Q.H., Li F.J. (2006). Scattering of Rayleigh waves by a shallow circular alluvial valley:

high-frequency solution. *ACTA Seimologica Sinica* (in Chinese) **28:2,** 176-182.

Liang J.W., Zhang Y.S., Gu X.L., et al. (2000). Surface motion of circular-arc layered alluvial valleys for incident plane SH waves. *Chinese Journal of Geotechnical Engineering* (in Chinese) **22:4,** 396-401.

Liang J.W., Yan L.J., Lee V.W. (2001). Scattering of plane P waves by circular-arc layered alluvial valleys: an analytical solution. *ACTA Seimologica Sinica* (in Chinese) **23:2,** 167-184.

Liang J.W., Yan L.J., Lee V.W. (2003). Diffraction of plane SV waves by a circular-arc layered alluvial valley: analytical solution. *ACTA Mechanica Solida Sinica* (in Chinese) **24:2,** 235-243.

Todorovska M.I. and Lee V.W. (1991). Surface motion of shallow circular alluvial valleys for incident plane SH wave-analytical solution. *Soil Dyn Earthq Engrg* **10:4,** 192-200.

Trifunac M.D. (1971). Surface motion of a semi-cylindrical alluvial valley for incident plane SH waves. *Bull Seism Soc Am* **61:6,** 1755-1770.

Wong H.L. and Trifunac M.D. (1974). Surface motion of a semi-elliptical alluvial valley for incident plane SH waves. *Bull Seism Soc Am* **64:5,** 1389-1403.

Yuan X.M. and Liao Z.P. (1995). Scattering of plane SH waves by a cylindrical alluvial valley of circular-arc cross-section. *Earthq Engrg Struct Dyn* **24,** 1303-1313.

Zhang Y.S. (2008). Analytical solution for the stationary response of alluvial valleys containing multiple circular-arc layers to incident plane P waves. Chinese J Geophys (in Chinese) **51:3,** 869-880.

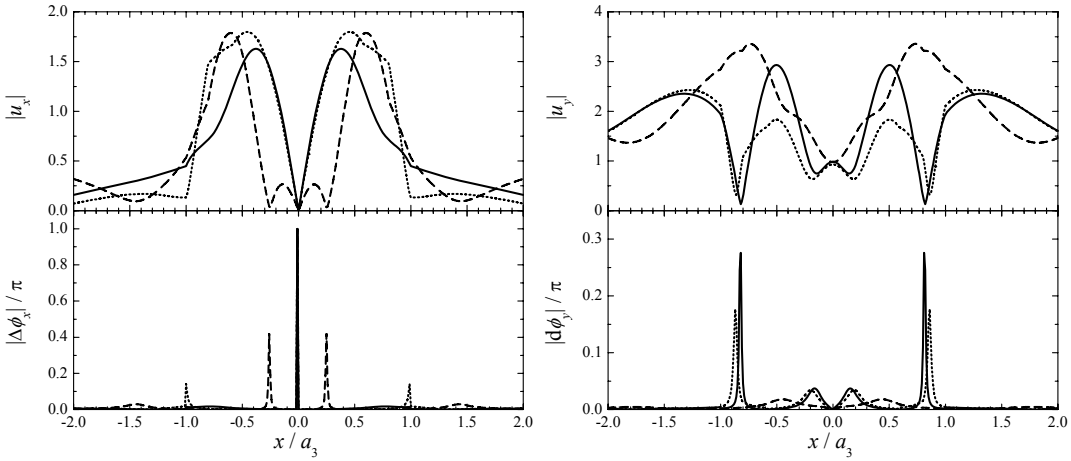


(a) $\eta = 1.0$

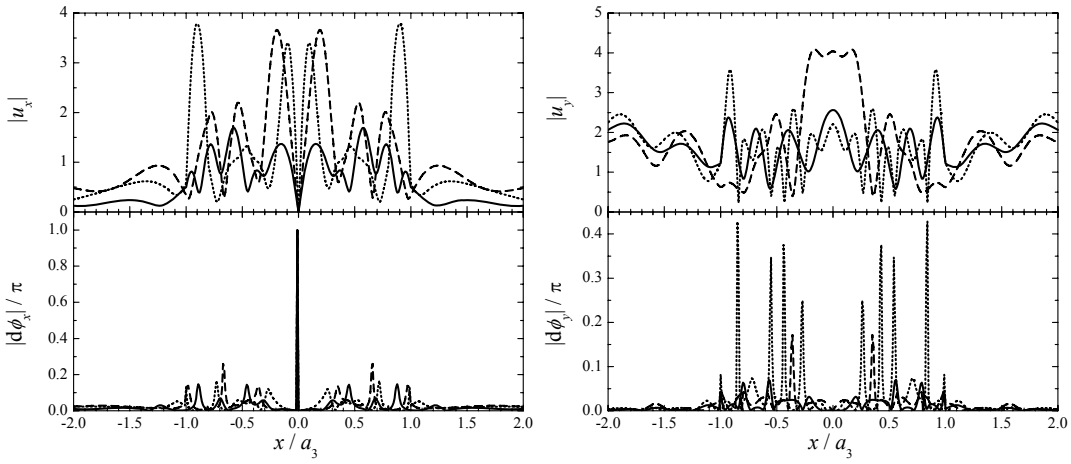


(b) $\eta = 4.0$

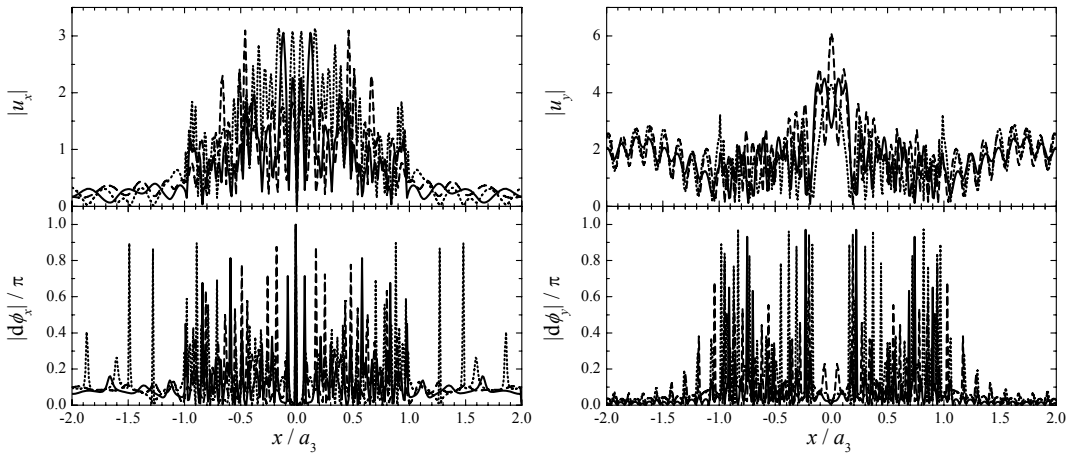


(c) $\eta = 16.0$

Figure 3 The case of vertical incidence (incident angle $\gamma_p = 0°$)
——— V-1; — — — V-2; ····· V-3

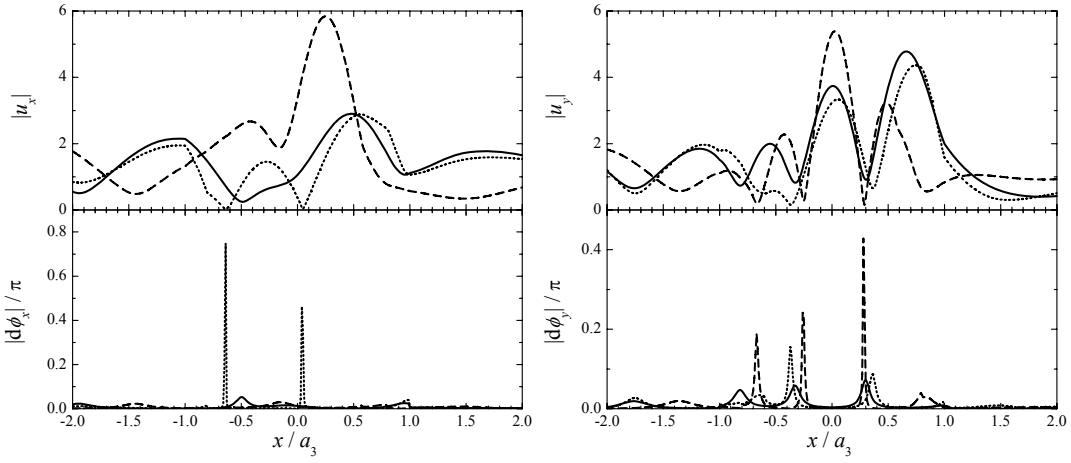


(a) $\eta = 1.0$

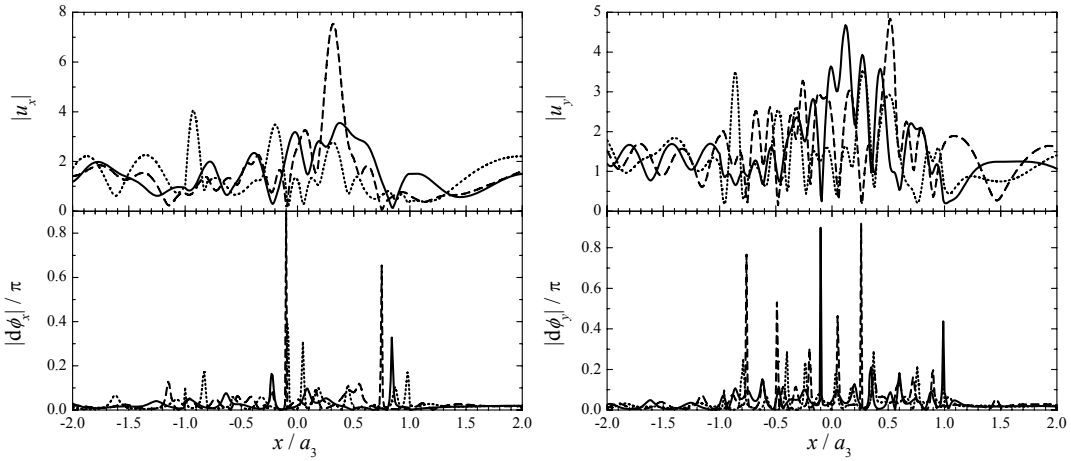


(b) $\eta = 4.0$

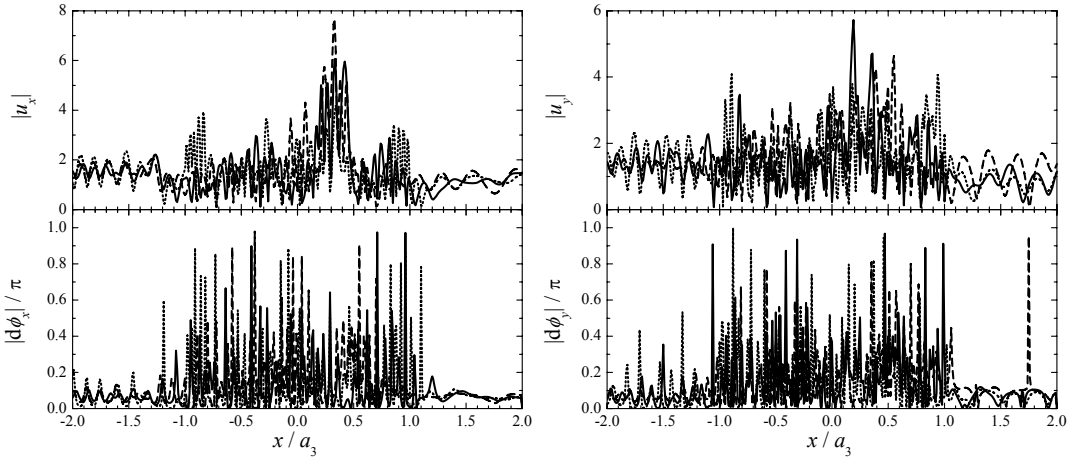


(c) $\eta = 16.0$

Figure 4 The case of inclined incidence (incident angle $\gamma_p = 45°$)
——— V-1; — — — V-2; ····· V-3